Numerical and Experimental Study of Cavitation Behaviour of a Propeller

Moustafa Abdel-Maksoud
Potsdam Model Basin (SVA)

1. Introduction

The prediction of the cavitation behaviour of a propeller is important to analyse the propeller in the design and off-design conditions. Water quality has a strong influence on the cavitation pattern. Therefore, in numerical as well as in experimental investigations, the quality of the water must be taken into account.

Skew propellers have many advantages, especially the reduction of cavitation and pressure pulses on the ship's stern. On the other hand, increasing the skew angle of the propeller increases the length of wall streamlines on the propeller blade. An accurate prediction of the viscous effects on the performance of the skew propeller is important, especially for off-design conditions.

The aim of this study is to investigate the aptitude of a general purpose cavitation model in calculating cavitation behaviour for ship propellers. In the experimental part of the study the cavitation pattern around a propeller model in off-design condition is measured and documented for different cavitation numbers. The computational part of the study includes the application of the cavitation model in CFX-TASCflow to calculate the flow characteristics on a propeller at each cavitation number.

2. Experimental Study

The experimental study was carried out in the cavitation tunnel of the Potsdam Model Basin for a five blade propeller model in homogeneous flow. The diameter of the propeller in model scale is 0.25 m. The scale ratio is $\lambda = 12$. Pitch ratio and blade area ratio are 1.635 and 0.779 respectively. The skew angle equals 18.8 degrees.

The cavitation behaviour of the propeller was observed at different cavitation numbers. The results are available as hand sketches, photos and video. The following cavitation numbers were considered in the study: 10.22, 9.58, 8.95, 8.32, 7.69, 7.05, 6.42, 5.79, 5.15, 4.52, 3.89, 3.26, 2.62, 1.99 and 1.36. The cavitation number is defined by the resultant flow velocity at 0.7 non-dimensional radius of the propeller blade. The thrust and the torque coefficients were also measured at each cavitation number.

3. Numerical computations

The periodicity of the propeller flow makes it possible to consider only one propeller blade in the computation. The influence of the other blades is taken into account by the application of periodic boundary condition in the space. The calculation domain is a 72 degrees segment of a cylinder.

The calculation domain is divided into a stationary part and a rotating part. A sliding boundary condition is applied between them. The propeller blade and a part of the propeller shaft are included in the rotating part of the calculation domain. In this part, a rotating co-ordinate system is applied to calculate the flow around the propeller.

The RANS equations in a rotating co-ordinate system involve additional terms compared to those in an inertial system. The computations were carried out using the commercial CFD software package CFX-TASCflow from AEA Technology. CFX-TASCflow uses a Finite Element based Finite Volume method. It uses block-structured non-orthogonal grids. CFX-TASCflow models the equations for the conservation of mass, momentum and energy in terms of the dependent variables velocity and pressure in their Reynolds averaged form. The variables are discretised on a co-located grid with a second order fully conservative vertex based scheme. In the computations the "Linear Profile" scheme with "Physical Advection Correction" of Schneider and Raw [1] was applied. The resulting linear equation system is solved with an Algebraic

Multi-Grid (AMG) solver, which shows a linear scalability of the code with the number of grid cells. The equations are solved fully coupled.

The standard k-ε turbulence model is applied in the present study in combination with a scalable wall function. The scalable near wall treatment allows a consistent grid refinement near the wall, Grotjans and Menter [2]. The applied cavitation model in the CFX-TASCflow is documented in detail in [3]. A short description of the cavitation model is given below.

3.1 Cavitation Model

When cavitation takes place, the mixture density of water and vapour can change rapidly with the formation of the vapour component. The component density, contrary to mixture one, does not change significantly. For the purpose of cavitation modelling it is desirable to re-cast the mass fraction conservation equation in terms of a volume-fraction equation, the benefit being that the mixture density no longer appears in the conservation equation.

The volume scalar equations are developed in the CFX-TASCflow method around the multi-component fluid (MCF) model. A MCF model has the capability to model fluid mixtures consisting of an arbitrary number of separate physical components (or ``species"). Each component fluid may have a distinct set of physical properties. The calculated average values of the properties of the mixture in each control volume in the flow domain will depend both on component property values and on the proportion of each component present in the control volume.

The volume fraction field may vary continuously from 0 to 1 in the cavitation zone covering many grid elements. The added complexity in comparison with the traditional VOF approach is that a source term is now added to the volume fraction equation to model the creation and destruction of vapour. This source term introduces a very strong coupling between the volume fraction equation and the mass, momentum equation set, since the source term depends on the local pressure difference. The resulting volume-fraction field strongly influences the mixture density used in the mass/momentum equations. It is this strong coupling that makes even the VOF cavitation model a difficult one to solve, most notably when the liquid/vapour density ratio becomes large (i.e. 1000 or larger).

Volume-Fraction Scalar Equations

The governing equations describe the cavitation process involving a two-phase three-component system, where it is assumed that no-slip between the phases takes place, and thermal equilibrium between all phases exists. The three components are:

1. Non-condensable gas in the form of micro-bubbles
2. Vapour (primary phase)
3. Liquid (primary phase)

The mass fraction of the non-condensable gas and the radius of the micro-bubbles have to be defined at the beginning of the computation.

The relative quantity of each of the components is described by a volume fraction scalar α. Particular volume fractions have the subscripts: d - dispersed, v - vapour in primary phase, and l - liquid in primary phase. The sum of all volume fractions must sum to one:

$$\alpha_d + \alpha_v + \alpha_l = 1 \qquad (1)$$

where the volume fractions are related to the mass fractions, y, for each component i through the relations:

$$y_i = \alpha_i \rho_i / \rho \qquad (2)$$

with the additional constraint that:

$$y_d + y_v + y_l = 1 \tag{3}$$

In the above relations, ρ_i is the density of the individual components (with $i = d$, v, and l) for the mixture when designated as ρ.

For the general cavitation case, compressibility in the vapour and liquid regions is important and therefore an equation of state is required to determine the density. Depending on the component considered, the equation of state required is:

- The density of the non-condensable component can be determined from an ideal gas equation of state using local pressure and temperature.
- The density of the primary phase vapour component can be treated as a constant (but evaluated at the saturation vapour pressure set by the free stream temperature).
- The density of the liquid component of the primary phase can be considered as a constant.

The solution of only two volume-fraction equations is needed, since the distribution of the third phase can be determined from Equation (1). In many cavitation problems the mass fraction associated with the non-condensable phase is assumed to be well mixed in the liquid phase with a constant y_d. On this basis the mass fractions y_l and y_d can be combined and treated as one. For this reason volume scalar α_m is introduced, where $\alpha_m = \alpha_l + \alpha_d$ and the density associated with α_m becomes ρ_m. The solution is carried for volume scalar α_m. The governing volume-fraction equation for the primary liquid phase with non-condensable gas becomes as follows:

$$\frac{\partial}{\partial t}(\rho_m \alpha_m) + \frac{\partial}{\partial x_j}(\rho_m u_j \alpha_m) = \dot{S}_l \tag{4}$$

The mass exchange between the vapour and liquid in the primary phases during cavitation is taken into account by the source terms $\dot{S}_l$ and $\dot{S}_v$, where $\alpha_v = 1 - \alpha_m$ and $\dot{S}_l = -\dot{S}_v$. The rate of vapour production of the source term $\dot{S}_v$ has been derived by considering the Rayleigh-Plesset equation (RPE) for bubble dynamics.

For a vapour bubble nucleated in a surrounding liquid the dynamic growth of the bubble can be described by the RPE as follows:

$$\dot{R}\ddot{R} + \frac{3}{2}\dot{R}^2 = \frac{p_v - p}{\rho_l} \tag{5}$$

where R is the radius of the bubble, p_v the vapour pressure in the bubble, p the pressure in the surrounding liquid and ρ_l the liquid density. In the applied cavitation model a first order approximation for RPE is used where:

$$\dot{R} = \sqrt{\frac{2}{3}\frac{p_v - p}{\rho_l}} \tag{6}$$

It is also assumed that there are no thermal barriers to the droplet growth. The bubbles growth takes place from an initial average radius of R_b and return (when condensing) to bubbles of the same size. The mass rate for vaporization and condensation of liquid can be calculated as follows:

$$\dot{S}_l = -\dot{S}_v = N\rho_v 4\pi R_b^2 \dot{R} \qquad (7)$$

where N is the number of bubbles per unit volume of the mixture , which are available as nucleation sites.

$$\dot{S}_l = -F_c N\rho_v 4\pi R_b^2 \dot{R}\sqrt{\frac{2}{3}\frac{p_v - p}{\rho_l}} sign(p_v - p) \qquad (8)$$

Since the volume fraction α_m is to be solved, representing well-mixed liquid and non-condensables, equation (8) is applied for the calculation of the vaporization and the condensation of liquid, which are the sink/source terms in equation (4).

In practice, the vaporization and condensation processes have different time scales, the condensation process typically being the slower one. An empirical constant, F_c is introduced in equation (8) to allow for these constraints:
with a typical value of $F_c = 50$ when vaporization occurs ($p_v - p > 0$) and $F_c = 0.01$ with condensation ($p_v - p < 0$). The factor F_c is a dimensionless value.

3.2 Numerical grid

A block structured grid is applied. The numerical grid contains 11 blocks. The number of control volumes in the numerical grid is 712.000. Figure 1 shows the topology of the numerical grid. The size of the tip vortex is very small in comparison to the size of the calculation domain. To calculate the pressure reduction in the tip vortex a local grid refinement was carried out. The number of control volumes after the refinement is 1.310.000. The results of the local refinement study on the pressure of the tip vortex region are presented in [4].

3.3 Boundary condition

The inflow velocity and the number of revolutions of the investigated operation point of the propeller are 5.625 m/s and 25 rps respectively. The turbulence degree was considered to be 3 %. The mass fraction of the non-condensable component was assumed to be 10^{-5} and the typical radius for the nucleation sites was 10^{-6} m.
An investigation of the influence of the water quality parameter on the calculated cavitation behaviour was out of scope of this study.

4. Results

4.1 Thrust and torque coefficients

The change of calculated and measured thrust and torque coefficients from the corresponding values without cavitation is shown as a function of the cavitation number in Figure 2. The calculated change of the thrust and of the torque coefficients follows the measured results. At high cavitation numbers some oscillation of the numerical results can be noticed. The drop of thrust at low cavitation number is well predicted. The experimental results show a small increase of the thrust and torque coefficients before the breaking down of the thrust. Similar behaviour can be seen in the numerical results. But the calculated increase of the coefficients is much less than those measured.

4.2 Velocity distribution

In a previous study, a comparison between the calculated and measured velocity components at the design condition of the propeller J = 1.245 was carried out. Figures 3 and 4 show the velocity distribution in the tip region of the propeller blade at the station 0.1D behind the propeller. The velocity components were normalised by the inflow velocity. The measurements were carried out using a non-coincident Laser Doppler Velocimeter. The comparison between the measured and the calculated values shows a good agreement of the axial and radial velocity components not only for the flow between the propeller blades but also for the flow behind them. The calculated tangential velocity component is somewhat higher than the measured values.

4.3 Cavitation patterns

The measured cavitation patterns are given in Figures 5 - 8 and those calculated in Figures 5 - 7. The photos in Figures 5 - 7 show the experimental results (in the left column). In the right column, the numerical results are included as graphics. The regions at which vapour takes place are visualised in shades of blue.

The measured and calculated results for σ = 1.36, 1.99 and 2.62 are included in Figure 5. At σ = 1.36, the measured cavitation pattern on the propeller shows a thick sheet of cavitating flow, which covers the propeller blade and the screw shaped surface of flow behind it. The calculated cavitation pattern shows the same behaviour. A good agreement could therefore be achieved. At this cavitation number, the thrust breaks down, the cavitation of hub vortex is no longer visible and the cavitation of the tip vortex is strongly reduced (see the experimental results).

The cavitation sheet on the propeller blade at σ = 1.99 is thinner and the cavitation of the hub vortex and the tip vortex are more visible than at σ = 1.36. This tendency has also been predicted by the numerical result.

Different types of cavitation can be seen at σ = 2.62. Suction side cavitation takes place up to the non-dimensional radius of r/R = 0.5. Root, leading edge, hub and tip vortex cavitation can be also seen in the experimental as well as in the numerical results.

Figure 6 shows the measured and calculated cavitation pattern at σ = 3.26, 3.89 and 4.52. At a cavitation number of 3.26, the blade area, which is subjected to suction side cavitation, is strongly reduced. The cavitation in the regions of leading edge and tip vortex is still intensive. The reduction of the root cavitation is over predicted in the numerical results. The same can be seen in the hub vortex. This is because the grid refinement was carried out only near the tip region. The grid resolution near the blade root is not adequate to predict the pressure reduction in this region. The numerical results still show root cavitation at σ = 3.89 and 4.52, but the volume of cavitating flow is very limited in comparison with the experimental results. At σ = 3.89 and higher it was not possible to predict any cavitation in hub vortex region due to the limited resolution of the numerical grid. The tip vortex cavitation is well calculated only on the propeller blade at σ = 3.89 and 4.52. This is because only the tip vortex region on the propeller blade is locally refined. Behind the propeller blade, where the coarse grid is located, it is not possible to predict the correct pressure reduction in the propeller slip stream.

Figure 7 includes the results for σ = 5.15, 5.79 and 6.42. The experimental results show that cavitation takes place in the tip, root and hub regions. Only tip vortex cavitation can be predicted by the numerical calculation. Above σ = 6.42 it was not possible to calculate any type of cavitation. The observed cavitation patterns at σ = 7.05, 7.69 8.32, 8.95, 9.58, 10.22 are given in Figure 8. It can be seen that hub vortex cavitation takes place at all investigated σ. By increasing the cavitation number the cavitation of the tip vortex moves away from the propeller blade tip to the propeller slip stream.

5. Conclusion

The propeller flow is characterised by very strong local velocity and pressure gradients. A good prediction of these gradients is very important in order to estimate the cavitation pattern on and behind a propeller blade. The applied cavitation model is able to predict most types of cavitation which take place in the propeller flow. The difficulty in prediction the cavitation at some of the cavitation numbers investigated is due to the lack of resolution of the numerical grid. It is possible to consider the effect of the water quality on the calculated cavitation pattern. More investigations on this subject are required to analyse the behaviour of the cavitation model.

6. Acknowledgement

The author would like to express his gratitude to Potsdam Model Basin GmbH and the staff of the Cavitation Department, Mr. H.-J. Heinke and D. Jaksic and Mrs. V. Kutterer for supporting his research, and carrying out the experimental part of the paper without any external funding.

7. Literature

[1] Schneider, G. E., Raw, M. J.
Control Volume Finite Element Method for Heat Transfer and Fluid Flow using Co-located Variables,
Numerical Heat Transfer, Vol. 11, pp. 363-390, 1987

[2] Grotjans, H., Menter, F. R.
Wall Functions for Industrial Applications,
Papailiou, K. D. Editor, Computational Fluid Dynamics 98, Volume 1, Part 2, pp.1112-1117, Chichester, 1998, ECCOMAS, John Wiley & Sons

[3] N. N.
User Documentation of CFX-TASCflow, version 02.12.00,
AEA-Technology GmbH, Otterfing, November 2002

[4] Abdel-Maksoud, M., Rieck, K.,
Calculation of the pressure reduction in the tip vortex core of a skew propeller in model and full-scale,
4th Numerical Towing Tank Symposium (NuTTS'01), Hamburg, September 2001

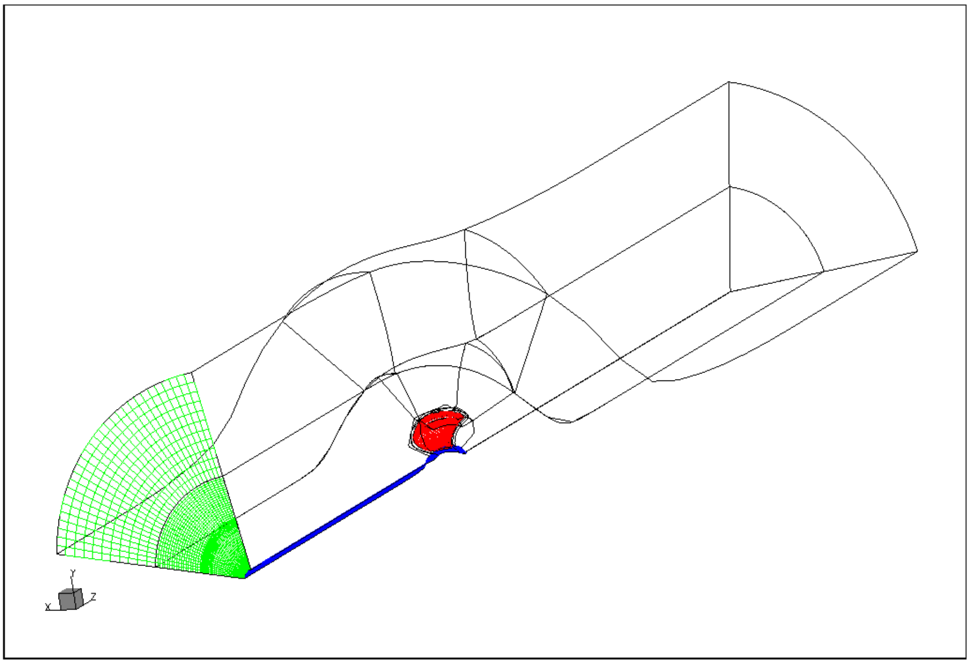

Figure 1: Topology of the numerical grid

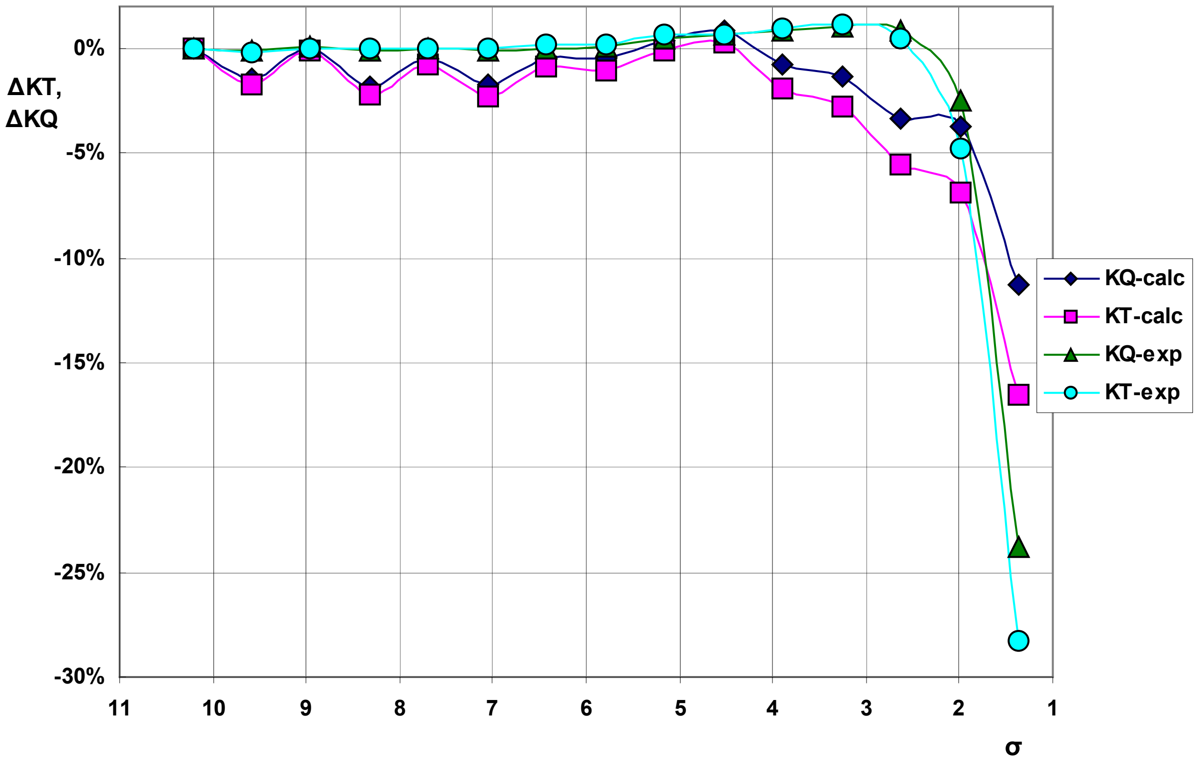

Figure 2: Change of the thrust and torque coefficients as a function of cavitation number

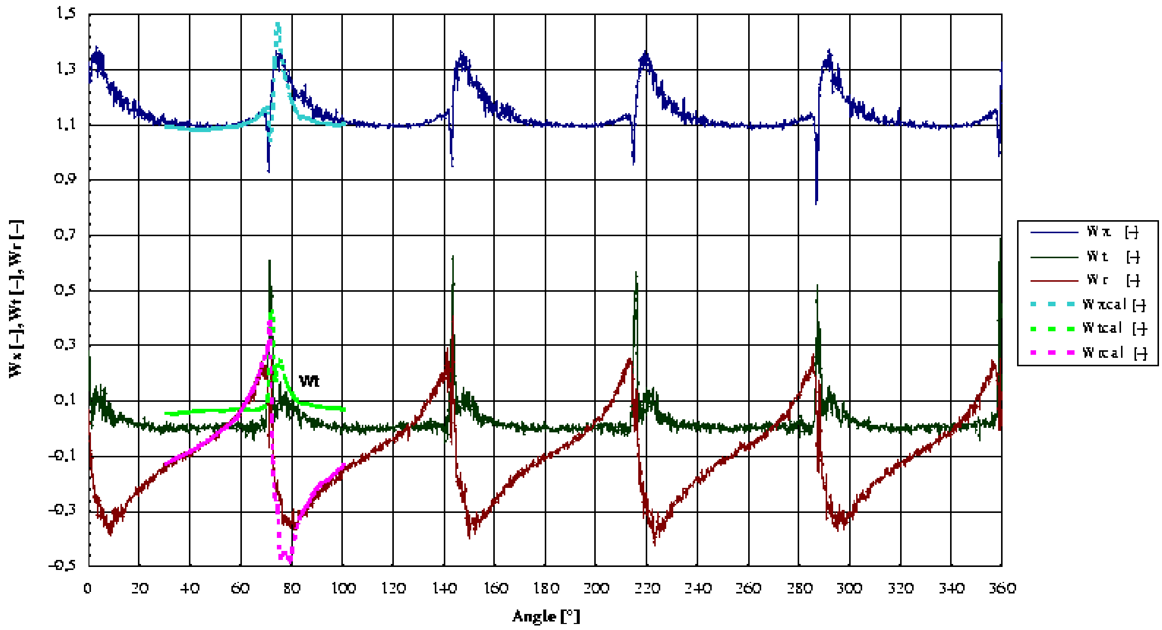

Figure 3: Measured and calculated velocity components, J = 1.245, x/D = 0.1, r/R = 0.95

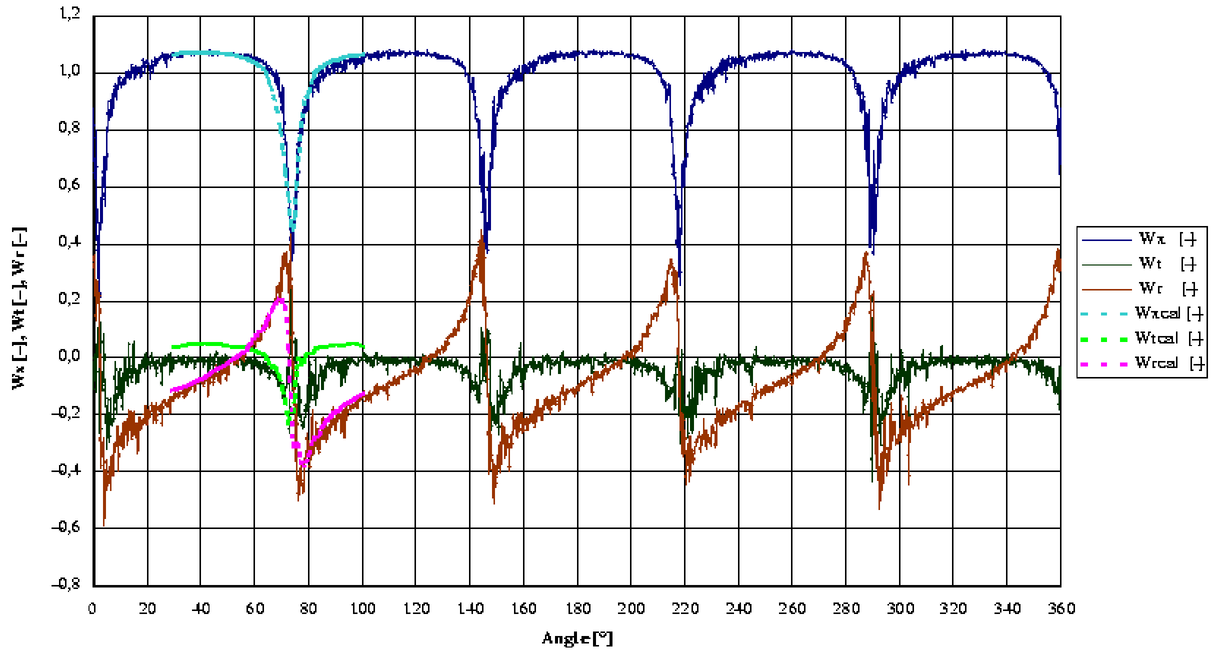

Figure 4: Measured and calculated velocity components, J = 1.245, x/D = 0.1, r/R = 1.0

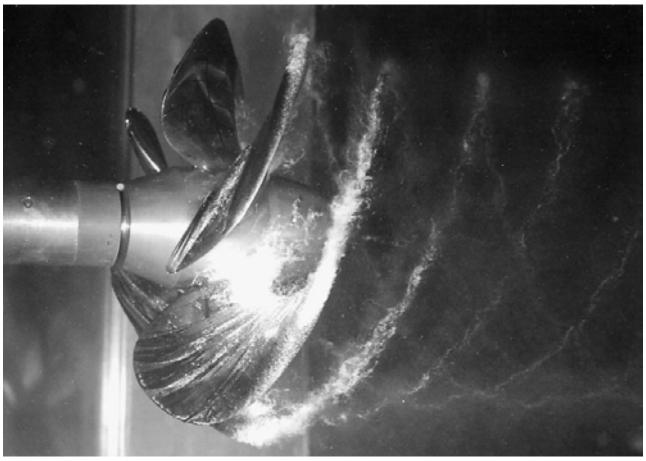
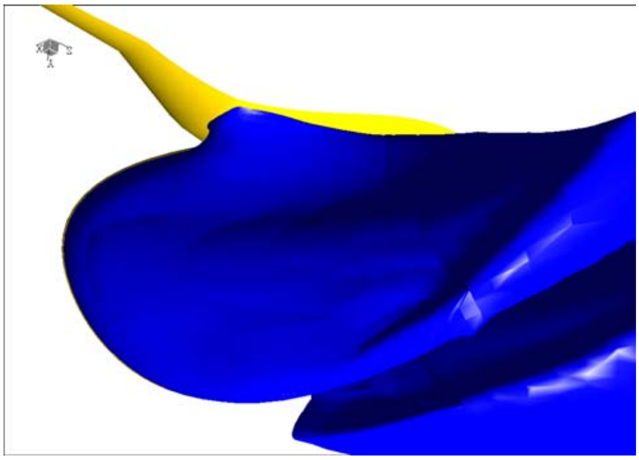

σ = 1.36

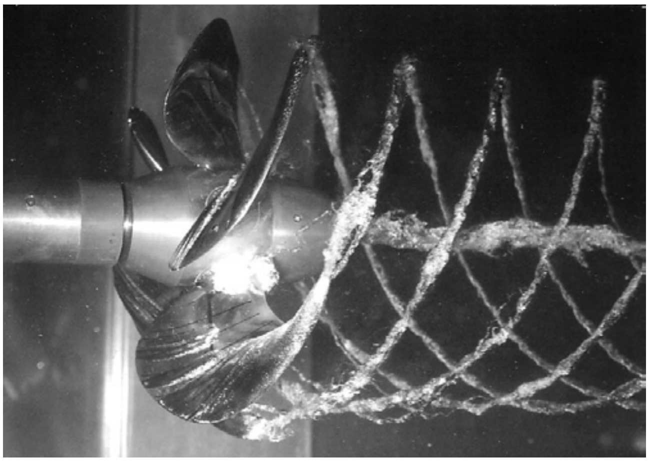
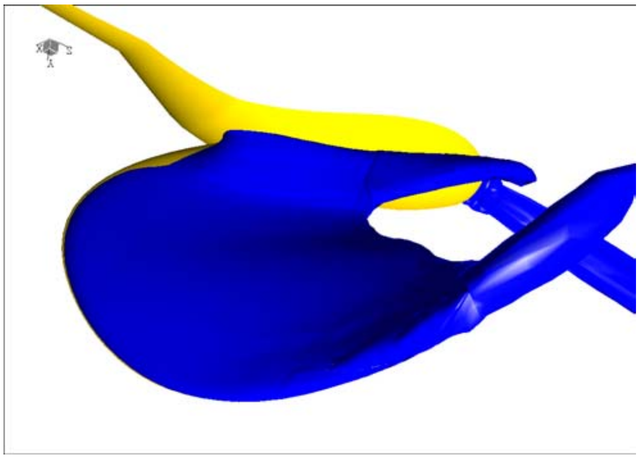

σ = 1.99

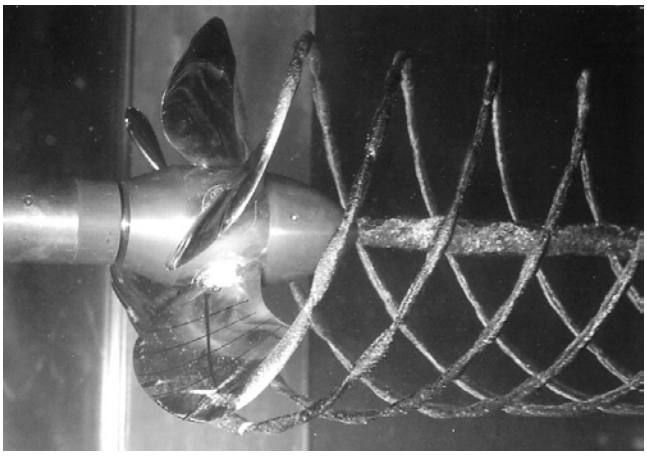
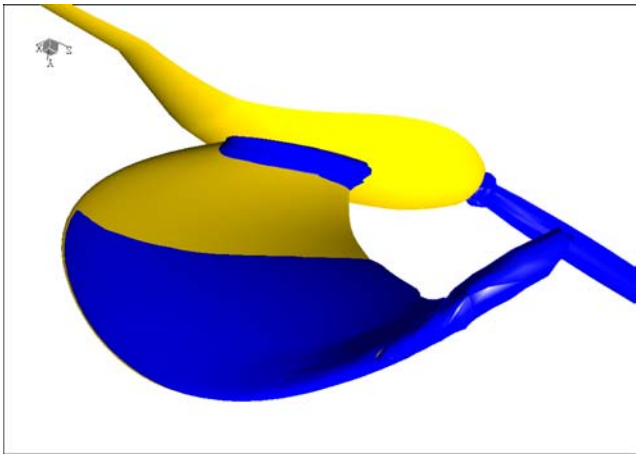

σ = 2.62

Figure 5: Comparison between measured and calculated cavitation behaviour, σ=1.36 -2.62

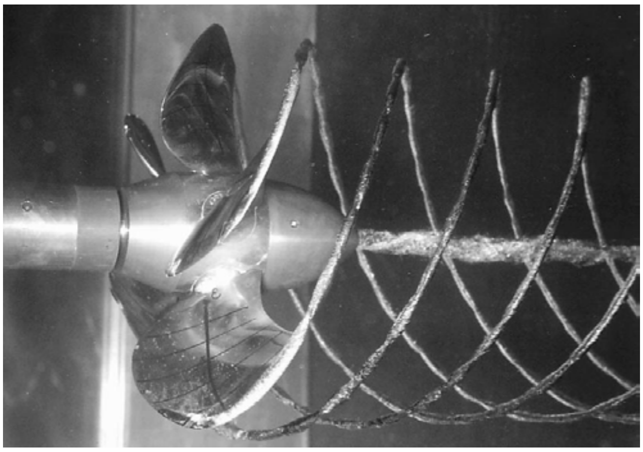
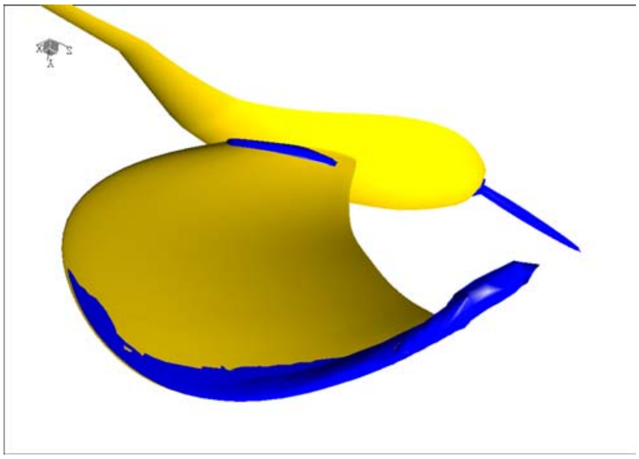

σ = 3.26

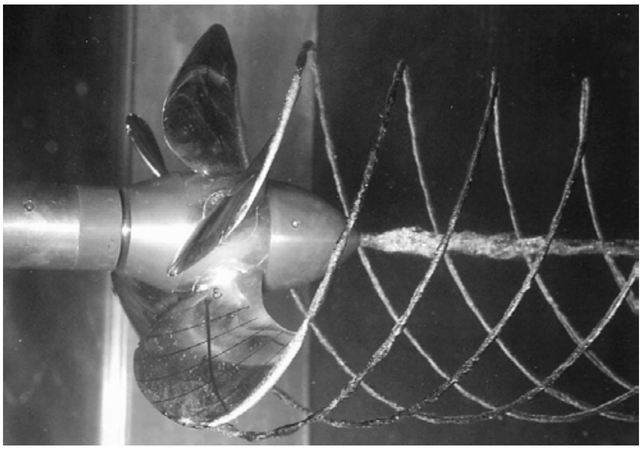
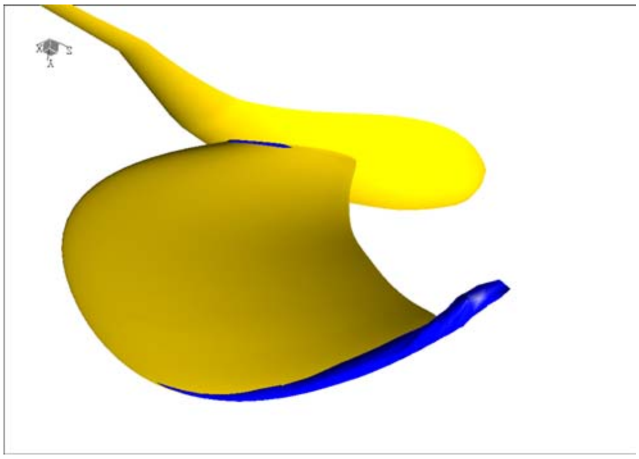

σ = 3.89

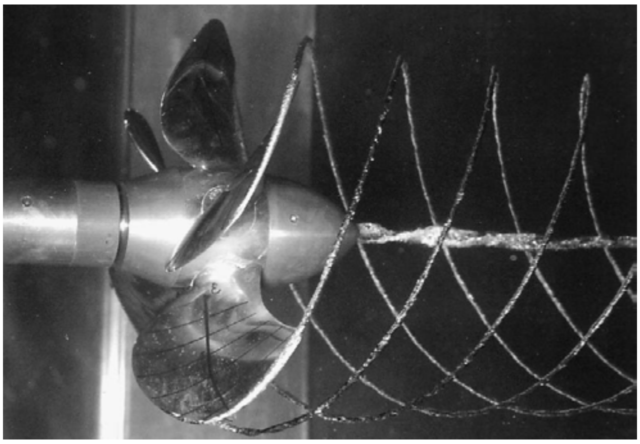
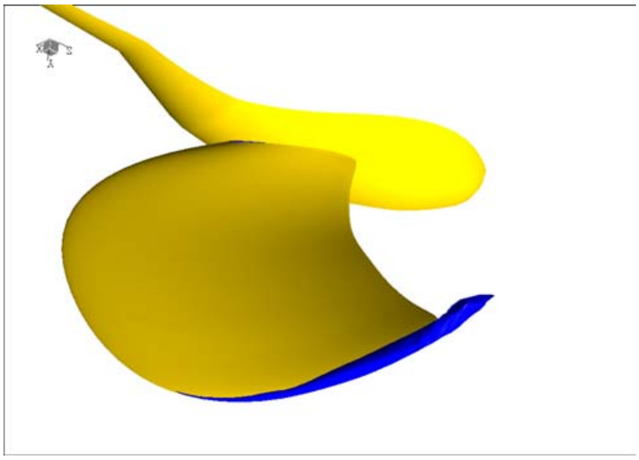

σ = 4.52

Figure 6: Comparison between measured and calculated cavitation behaviour, σ = 3.26 - 4.52

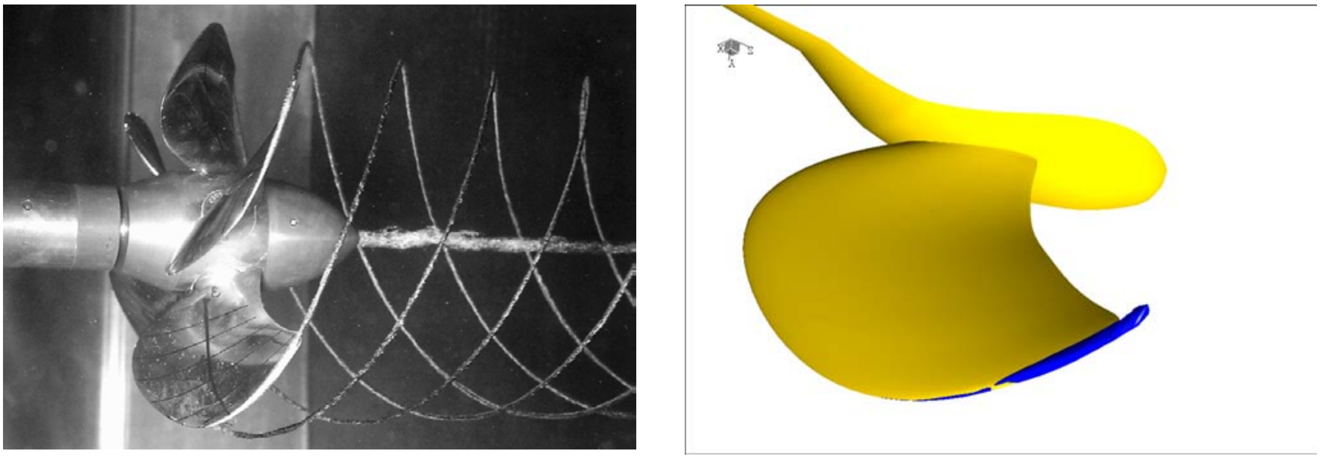

σ = 5.15

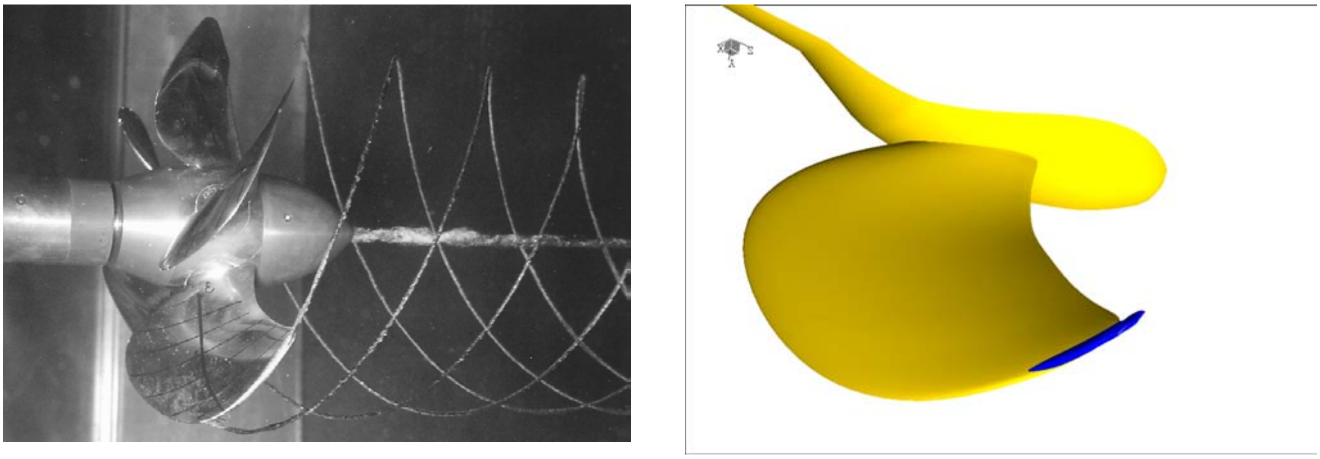

σ = 5.79

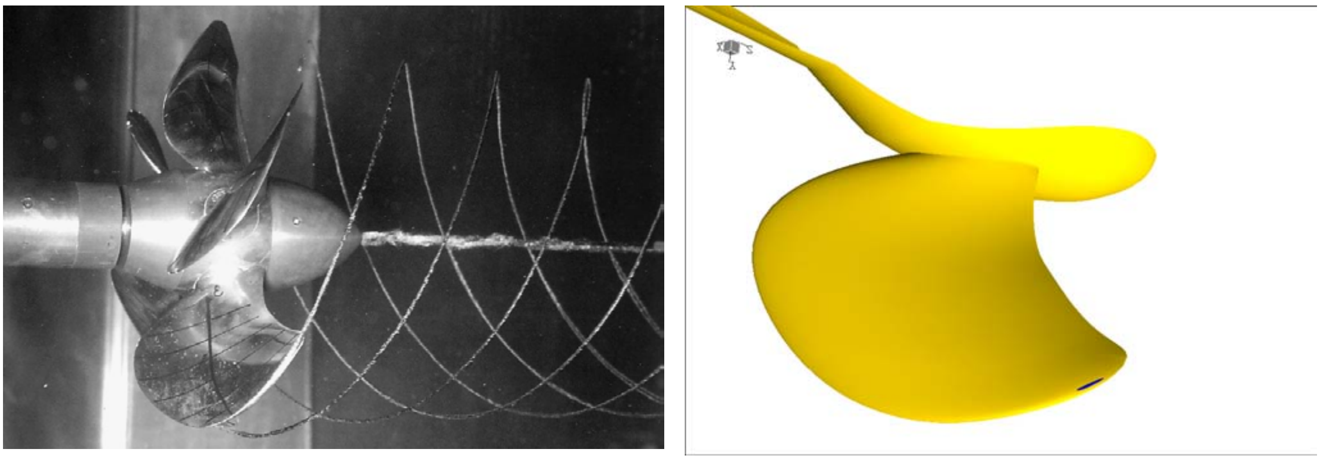

σ = 6.42

Figure 7: Comparison between measured and calculated cavitation behaviour, σ = 5.15 - 6.42

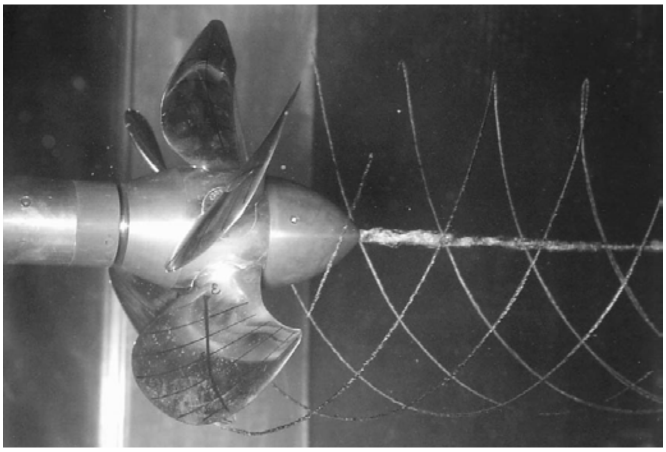
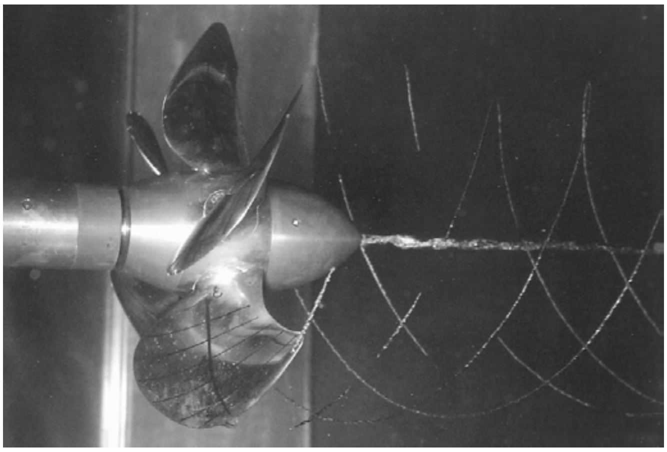

σ = 7.05　　σ = 7.69

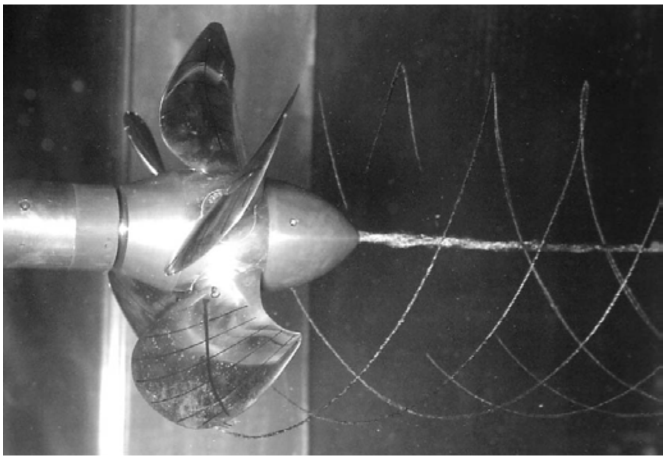
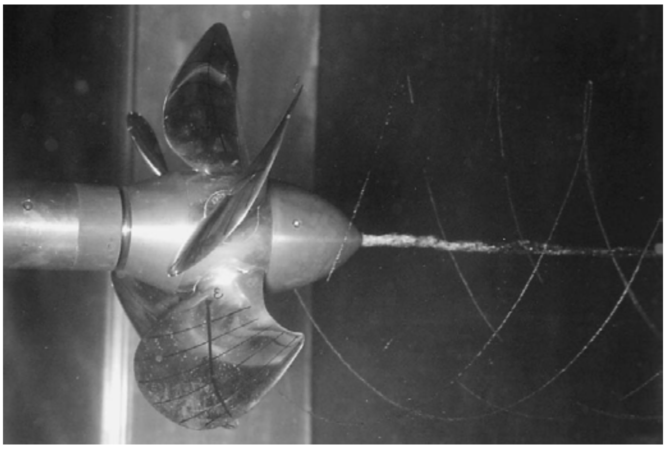

σ = 8.32　　σ = 8.95

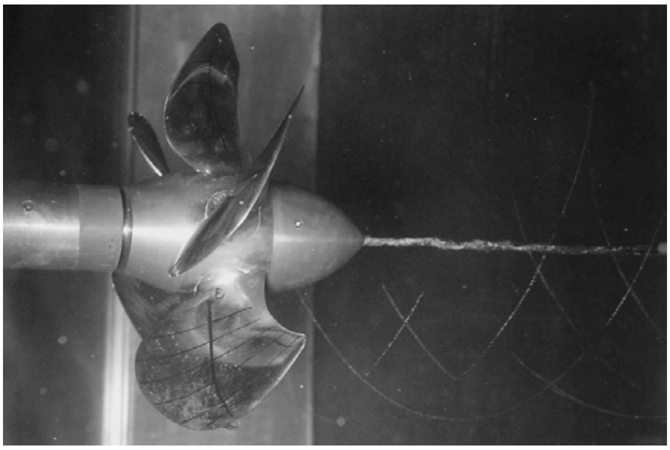
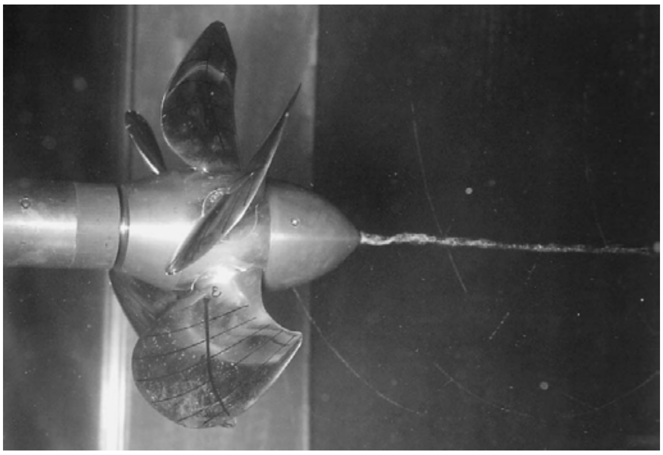

σ = 9.58　　σ = 10.22

Figure 8: Measured cavitation behaviour, σ = 7.05 - 10.22